J. Appl. Comput. Mech., 11(3) (2025) 844-860
DOI: 10.22055/jacm.2024.47901.4824

ISSN: 2383-4536
jacm.scu.ac.ir

Shahid Chamran
University of Ahvaz

Journal of
Applied and Computational Mechanics

Research Paper

A Very High-Order Spatial Lagrange Interpolating Polynomial Scheme

Uthai Prasopchingchana

Department of Mechanical Engineering, Burapha University, Chonburi, 20131, Thailand, Email: uthai@eng.buu.ac.th

Received September 08 2024; Revised November 12 2024; Accepted for publication November 16 2024.
Corresponding author: U. Prasopchingchana (uthai@eng.buu.ac.th)

Abstract. This paper presents the extension of the Lagrange Interpolating Polynomial (LIP) scheme for solving differential equations by using the finite volume method called the Very high-order Spatial Lagrange Interpolating Polynomial (VS-LIP) scheme. The advantage of the VS-LIP scheme is its convenience for extending the order of accuracy. The correctness of the VS-LIP scheme solutions is assessed by comparing the solutions with analytical, benchmark, published, and experimental solutions of five verification problems involving one- and two-dimensional heat transfer and fluid flow. The assessment is carried out to the sixth and twelfth orders of spatial accuracy. The assessment results indicated that the VS-LIP scheme delivers the correct solutions.

Keywords: Very high-order Spatial Lagrange Interpolating Polynomial scheme; finite volume method; heat conduction; natural convection; lid-driven cavity flow.

1. Introduction

Using very high-order schemes (The accuracy is greater than the fourth order) [1-4] to solve scientific and engineering problems has elicited interest from many researchers because of their accurate solutions. In addition, the development of higher-performance computers has reduced the required computational time. Multiple very high-order schemes have been proposed in the last decade. Most were developed as extensions of classical second-order or high-order schemes. Gerolymos et al. [1] extended the Weighted Essentially Non-Oscillatory order (WENO) scheme into a very high-order WENO scheme to solve problems involving hyperbolic conservation laws. Numerous authors later proposed sixth-order schemes for spatial discretization [2, 5-12]. Wu et al. [13] reported a very high-order WENO scheme with new smoothness indicators. These new schemes displayed better behavior near critical points and better stability near discontinuities compared to the classical schemes. Jiang et al. [14] reported a very high-order implicit large eddy simulation developed from the seventh-order dissipative compact scheme. Clain and Machado [3] presented the extended Butcher tableau for temporal discretization up to eighth-order accuracy. Mazaheri and Nishikawa [15] constructed a very high-order hyperbolic scheme for temporal discretization up to the sixth order. Fu [16] proposed a very high-order Targeted Essentially Non-Oscillatory (TENO) scheme and assessed the performance at eighth-order accuracy by simulations of incompressible and compressible problems. The results demonstrated that the TENO scheme was robust and stable. Fu [4] improved the family of very high-order TENO schemes by adding adaptive accuracy order and adaptive dissipation control to upgrade the performance for fluid simulations. A solution set of benchmark problems was employed to demonstrate the performance of the improved TENO schemes, and they showed good robustness for conventional gas dynamics. Vasconcelos et al. [17] proposed a very high-order finite volume method based on the weighted least-squares method and simulated on unstructured grids to determine the solutions of the Poisson equation. An efficiency test showed that the eighth-order scheme was more computationally efficient than lower-order schemes. Very high-order schemes have also been extended to the medical sciences. For example, Coudière and Turpault [18, 19] adopted a very high-order finite volume method to simulate the propagation of electrical signals in the heart. Bai and Zhong [20] presented a very high-order upwind multi-layer compact scheme for flow simulations on structured grids. New schemes up to the seventh order were derived in the finite difference framework. Computational efficiency tests indicated that the new schemes delivered solutions with very high-order accuracy. Gaburro et al. [21] proposed a new family of very high-order schemes called direct arbitrary Lagrangian-Eulerian finite volume and discontinuous Galerkin schemes, which they used to solve nonlinear hyperbolic partial differential equations. They numerically verified the new schemes with second- to fifth-order accuracy in both space and time for smooth problems. A large set of benchmark problems in hydrodynamics and magnetohydrodynamics was employed to demonstrate the accuracy and robustness of the new schemes. Tsoutsanis and Dumbser [22] extended the Central WENO (CWENO) and CWENO-Z (CWENOZ) schemes to present very high-order central non-oscillatory schemes with up to sixth-order spatial accuracy. They tested the novel schemes on 2D and 3D problems, and the results indicated improved robustness. Guo et al. [23] presented a very high-order finite volume compact scheme, which they used to solve the one-dimensional Burgers' equation. The new scheme displayed strong stability and gave more accurate solutions than some numerical solutions in the literature. Xu [24] devised a very high-order scheme using the finite volume method for solving unsteady heat conduction problems. Its solutions were compared to

Published online: December 05 2024

the 1D, 2D, and 3D numerical solutions and analytical solutions (exact solutions), and the scheme exhibited better performance than the high-order compact finite difference method and Runge–Kutta discontinuous Galerkin method. Costa and Albuquerque [25] detailed a novel approach toward temporal simulations using very high-order finite volume schemes, where the Crank–Nicolson scheme was used for temporal discretization. They verified their approach for fourth-, sixth-, and eighth-order accuracy in the 1D and 2D unsteady cases. They verified the novel scheme up to the eighth order in both Cartesian and unstructured meshes. The scheme delivered faster and more accurate results than the second-order scheme. Recently, a mean preserving moving least squares method was proposed by Ramírez et al. [26]. The proposed method was developed for arbitrary order schemes of the finite volume method. The assessment of the proposed method in both accuracy and performance was carried out by using several benchmark problems. The assessment results showed that an arbitrary order of convergence could be achieved.

Some researchers [27-30] approximated the values and derivative values of equations by using polynomial interpolation methods. Previously, Prasopchingchana worked with Manewattana [30] to introduce a high-order temporal and spatial scheme called the Lagrange Interpolating Polynomial (LIP) scheme. The strategy of the difference between the LIP scheme and the other polynomial interpolation methods is that the specific point used to determine the interpolated value is imposed to be zero. Additionally, they demonstrated the mathematical proving for the accuracy order of the scheme. This scheme can easily be extended to a very high order by rewriting the letter notation to numerical notation. This article presents the extension of the LIP scheme called the Very high-order Spatial Lagrange Interpolating Polynomial (VS-LIP) scheme. Consequently, solutions obtained from the VS-LIP scheme are more accurate than those obtained from the LIP scheme.

The rest of the article is organized as follows: Section 2 details the VS-LIP scheme. Section 3 presents the problems used to verify the VS-LIP scheme and their solutions. Section 4 offers some perspectives on the VS-LIP scheme and concludes the article.

2. Mathematical Model of the VS-LIP Scheme

The VS-LIP scheme rewrites the notation for the LIP scheme, which is based on the finite volume method and rectangular cells. In the LIP scheme, the values of variables (ϕ) on the western, eastern, southern, and northern cell faces are expressed as $(\phi_{nt,i,j})_w$, $(\phi_{nt,i,j})_e$, $(\phi_{nt,i,j})_s$, and $(\phi_{nt,i,j})_n$, respectively. In the VS-LIP scheme, the values of the variables on the cell faces can be written as $\left(\phi_{nt,i1,i2}\right)_{na,nf}$ instead. Then, the coordinate axes and spaces in domains are expressed as x_{na} and $(x_{na})_{nf,i(na)}$, respectively. Table 1 presents the detailed notation. The values of variables at the center of cells can be written in a short form as $\phi_{nt,i1,i2}$, and the values of $nch(na,nf,i(na))$ in Table 1 can be calculated under any constraints indicated in Appendix A.

Figure 1 shows the temporal and 2D spatial axes of a problem domain with cells conforming to the VS-LIP scheme. The abbreviations C, w, e, s, and n are the cell center, the western, eastern, southern, and northern cell surfaces, respectively. The values and derivative values of variables on all cell faces with respect to space at the present time are written as:

$$\left(\phi_{ntmax,i1,i2}\right)_{na,nf} = \sum_{nc=1}^{ncmax(na)} \left(LX_{na,nf,i(na),nc}\ \phi_{ntmax,i1+ncc1,i2+ncc2}\right) \tag{1}$$

where

$$\begin{cases} na=1,\ nf=1,2 \text{ and } 1\le nc\le ncmax(1) \rightarrow \text{Constraint-1} \\ na=2,\ nf=1,2 \text{ and } 1\le nc\le ncmax(2) \rightarrow \text{Constraint-2} \end{cases}$$

$$\text{Constraint-1} = \begin{cases} ncc1 = nc - nch(1,nf,i1) \\ ncc2 = 0 \end{cases}$$

$$\text{Constraint-2} = \begin{cases} ncc1 = 0 \\ ncc2 = nc - nch(2,nf,i2) \end{cases}$$

and

$$\frac{d\left(\phi_{ntmax,i1,i2}\right)_{na,nf}}{d(x_{na})} = \sum_{nc=1}^{ncmax(na)} \left(DLX_{na,nf,i(na),nc}\ \phi_{ntmax,i1+ncc1,i2+ncc2}\right) \tag{2}$$

where

$$\begin{cases} nf=0 \begin{cases} i=icmin \text{ or } i=icmax \begin{cases} na=1, \text{ and } 1\le nc\le ncmax(1)\rightarrow \text{Constraint-1} \\ na=2, \text{ and } 1\le nc\le ncmax(2)\rightarrow \text{Constraint-2} \end{cases} \\ icmin<i<icmax \begin{cases} 1\le nc<nch(na,0,i(na)) \begin{cases} na=1 \rightarrow \text{Constraint-1} \\ na=2\rightarrow \text{Constraint-2} \end{cases} \\ nch(na,0,i(na))\le nc\le ncmax(na) \begin{cases} na=1\rightarrow \text{Constraint-3} \\ na=2\rightarrow \text{Constraint-4} \end{cases} \end{cases} \end{cases} \\ nf=1,2 \begin{cases} na=1, \text{ and } 1\le nc\le ncmax(1)\rightarrow \text{Constraint-1} \\ na=2, \text{ and } 1\le nc\le ncmax(2)\rightarrow \text{Constraint-2} \end{cases} \end{cases}$$

$$\text{Constraint-3} = \begin{cases} ncc1 = 1 + nc - nch(1,0,i1) \\ ncc2 = 0 \end{cases}$$

$$\text{Constraint-4} = \begin{cases} ncc1 = 0 \\ ncc2 = 1 + nc - nch(2,0,i2) \end{cases}$$

Table 1. Notation and definitions.

Abbreviation	Meaning	Value
nt	Numbers of time steps	$1 \le nt \le ntmax$ where *ntmax* is the present time step. $ntmax = 4$
na	Axis numbers	$na = 1$ (The horizontal axis) $na = 2$ (The vertical axis)
nf	Face numbers of cells	$nf = 0$ (The center of cells) $nf = 1$ (Western or southern faces of cells) $nf = 2$ (Eastern or northern faces of cells)
i(*na*)	Spatial grid numbers along the *na* axis	$i(na) = i(1) = i1$ (Grid numbers in the horizontal direction) $i(na) = i(2) = i2$ (Grid numbers in the vertical direction)
nc	Numbers of cells for approximation	$1 \le nc \le ncmax(na)$ where *ncmax*(*na*) is the spatial order of the VS-LIP scheme along the *na* axis. $ncmax(na)$ = an even integer ≥ 2
nch (*na*, *nf*, i(*na*))	Location numbers of the central cell in *ncmax*(*na*) on the cell face *nf* and at the grid number i(*na*).	$1 \le nch(na, nf, i(na)) \le ncmax(na)$

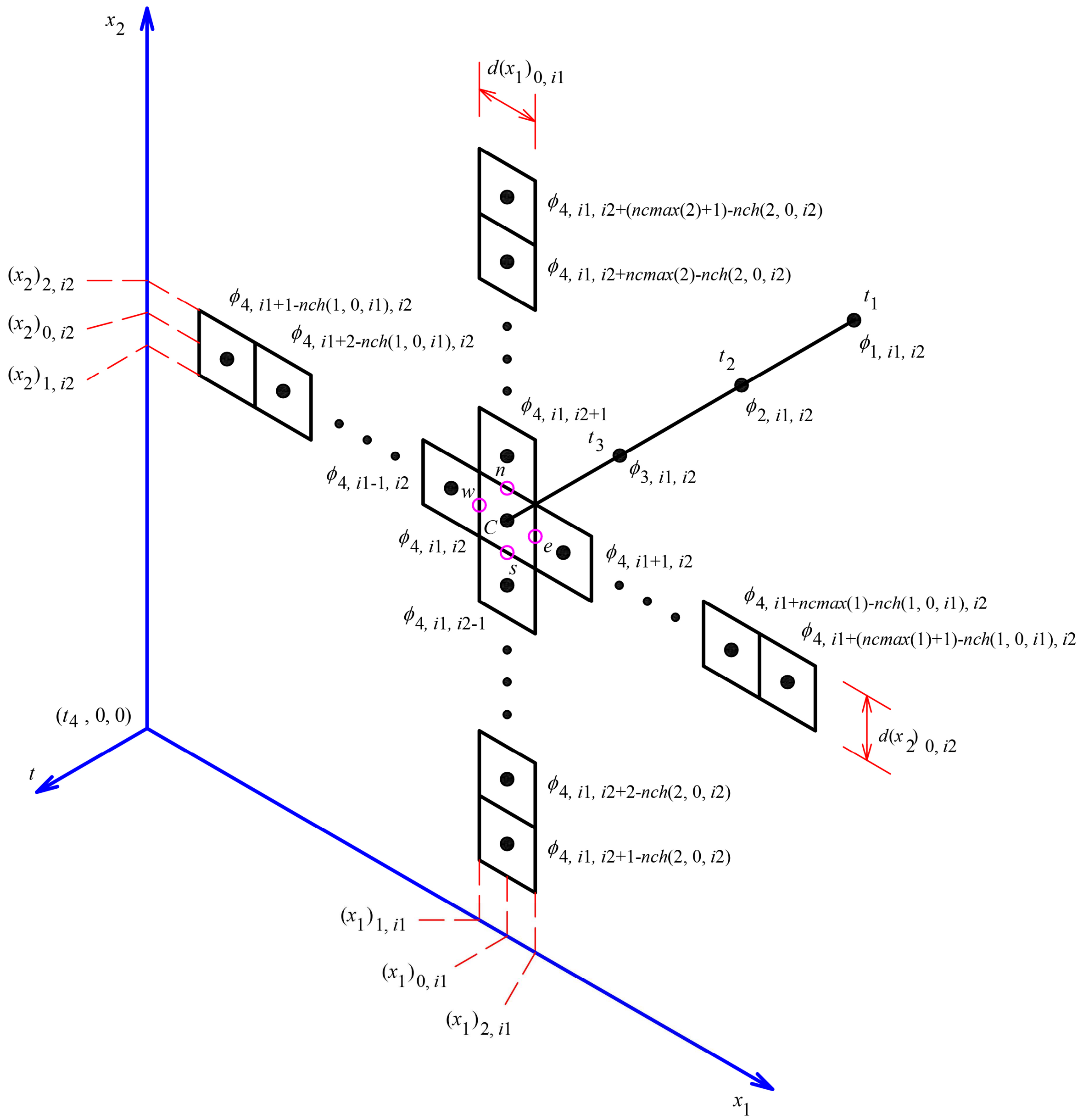

Fig. 1. Schematic of the VS-LIP scheme.

Table 2. Spatial coefficient and the temporal and derivative coefficients of the VS-LIP scheme.

Coefficient and derivative coefficient	Definition
$LX_{na,\,nf,\,i(na),\,nc} = \prod_{\substack{ii=1\\ ii\neq nc}}^{ncmax(na)} \frac{\left(-(X_{na})_{nf,\,i(na),\,ii}\right)}{\left((X_{na})_{nf,\,i(na),\,nc} - (X_{na})_{nf,\,i(na),\,ii}\right)}$	$(X_{na})_{nf,\,i(na),\,nc} = (x_{na})_{0,\,i(na)+ncc(na)} - (x_{na})_{nf,\,i(na)}$ $na = 1, 2$ $nf = 1, 2$ $nc = 1, 2, \cdots, ncmax(na)$ $ncc(na) = nc - nch(na, nf, i(na))$
$DLT_{nt} = \frac{\sum_{\substack{m=1\\ m\neq nt}}^{ntmax} \left(\prod_{\substack{mm=1\\ mm\neq m\\ mm\neq nt}}^{ntmax} (-TT_{mm}) \right)}{\prod_{\substack{m=1\\ m\neq nt}}^{ntmax} (TT_{nt} - TT_{m})}$	$TT_{nt} = t_{nt} - t_{ntmax}$ $nt = 1, 2, \cdots, ntmax$
$DLX_{na,\,nf,\,i(na),\,nc} = \frac{\sum_{\substack{ii=1\\ ii\neq nc}}^{ncmax(na)} \left(\prod_{\substack{iii=1\\ iii\neq ii\\ iii\neq nc}}^{ncmax(na)} \left(-(X_{na})_{nf,\,i(na),\,iii}\right) \right)}{\prod_{\substack{ii=1\\ ii\neq nc}}^{ncmax(na)} \left((X_{na})_{nf,\,i(na),\,nc} - (X_{na})_{nf,\,i(na),\,ii}\right)}$	$(X_{na})_{nf,\,i(na),\,nc} = (x_{na})_{0,\,i(na)+ncc(na)} - (x_{na})_{nf,\,i(na)}$ $na = 1, 2$ $nf = 0, 1, 2$ $nc = 1, 2, \cdots, ncmax(na)$ $ncc(na) = nc - nch(na, nf, i(na))$

where *LX* and *DLX* are the spatial coefficient and spatial derivative coefficient of the VS-LIP scheme. The derivative values of the variables with respect to the present time are written as follows:

$$\frac{d\phi_{ntmax,\,i1,\,i2}}{dt} = \sum_{nt=1}^{ntmax} \left(DLT_{nt}\ \phi_{nt,\,i1,\,i2} \right) \tag{3}$$

where *t* and *DLT* are the time and temporal derivative coefficient of the VS-LIP scheme, respectively. Table 2 presents the algebraic forms of the spatial coefficient and the temporal and spatial derivative coefficients of the VS-LIP scheme modified from [31].

3. Assessment of the VS-LIP Scheme

To assess the VS-LIP scheme, in-house codes are developed to solve five problems:

- Unsteady one-dimensional heat conduction,
- Steady-state two-dimensional heat conduction,
- One-dimensional Burgers' equation,
- Lid-driven cavity flow, and
- Natural convection in a rectangular cavity.

The VS-LIP scheme is used to obtain the solutions of the problems in the steady-state condition by approaching with transient governing equations. The VS-LIP solutions are compared with previously reported analytical, benchmark, published, and experimental solutions.

3.1. "Unsteady One-Dimensional Heat Conduction" Problem

Unsteady one-dimensional heat conduction is defined by:

$$\frac{\partial T}{\partial t} - (\nabla \cdot \nabla) T = 0 \tag{4}$$

where *T* is the temperature. The del operator is $\nabla = \partial/\partial x$, and *x* is the space. The domain of the problem, initial condition, boundary condition, and exact solution [24] are, respectively, expressed as:

$$x \in [0, 2\pi]\,,\ T(0,x) = \sin x\,,\ T(t,0) = T(t,2\pi) = 0\,,\ \text{and}\ \ T(t,x) = e^{-t} \sin x \tag{5}$$

Equation (4) is integrated for the finite volume of the central cell:

$$\int_{CV} \left(\frac{\partial T}{\partial t} \right) d\forall - \int_{CV} \left((\nabla \cdot \nabla) T \right) d\forall = 0 \tag{6}$$

where CV is the control volume of the cell. Then, Gauss's divergence theorem is applied to Eq. (6):

$$\int_{CV} \left(\frac{\partial T}{\partial t} \right) d\forall - \int_{CS} \left((\mathbf{n} \cdot \nabla) T \right) dA = 0 \tag{7}$$

where CS and **n** are the control surface and unit vector normal to the cell faces, respectively. Then, Eq. (7) is expanded to:

$$\frac{\partial T}{\partial t} d(x)_C - \left(\left(\frac{\partial T}{\partial x} \right)_e - \left(\frac{\partial T}{\partial x} \right)_w \right) = 0 \tag{8}$$

Table 3. Relative L^2 error obtained from the one-dimensional unsteady heat conduction problem with sixth and twelfth-order accuracies.

Total number of grid points	Relative L^2 error		
	6th Order accuracy	12th Order accuracy	Difference
20	1.0147E-02	1.0130E-02	1.7E-05
30	4.2768E-03	4.2760E-03	8.0E-07
40	2.3469E-03	2.3467E-03	2.0E-07
50	1.4805E-03	1.4804E-03	1.0E-07

The VS-LIP scheme is used to discretize the derivative values of the temperature with respect to time and space on the central cell and cell faces, respectively. Therefore, the temperature distribution can be derived as:

$$\left(\sum_{nt=1}^{ntmax}\left(DLT_{nt}\,T_{nt,\,i1}\right)d(x_1)_{0,\,i1}\right)-\sum_{nf=1}^{2}\left((-1)^{nf}\sum_{nc=1}^{ncmax(1)}\left(DLX_{1,\,nf,\,i1,\,nc}T_{ntmax,\,i1+ncc1}\right)\right)=0 \tag{9}$$

Equation (9) can be rearranged to:

$$T_{ntmax,\,i1}=\frac{\left(-\sum_{nt=1}^{ntmax-1}\left(DLT_{nt}\,T_{nt,\,i1}\right)d(x_1)_{0,\,i1}+\sum_{nf=1}^{2}\left((-1)^{nf}\sum_{nc=1}^{ncmax}\left(DLX_{1,\,nf,\,i1,\,nc}T_{ntmax,\,1i+ncc1}\right)\right)\Big|\text{When } ncc1\neq 0\right)}{\left(DLT_{ntmax}\,d(x_1)_{0,\,i1}-\sum_{nf=1}^{2}\left((-1)^{nf}\sum_{nc=1}^{ncmax}\left(DLX_{1,\,nf,\,i1,\,nc}\right)\right)\Big|\text{When } ncc1=0\right)} \tag{10}$$

The relative L^2 error [24] is used to assess the VS-LIP scheme for this problem. The relative L^2 error is defined as $(\sqrt{\int_L (T_n - T_e)^2 dS}/(\int_L T_e^2 dS)$, where T_n and T_e are the numerical and exact solutions, respectively. The letter S is the length of the spatial domain, and the time step is equal to $1/G$, where G is the total number of grid points. Table 3 presents the relative L^2 error of the VS-LIP scheme. The relative L^2 error is computed at $t = 1$. The relative residual error for numerical and exact solutions is 10^{-10}.

3.2. "Steady-State Two-Dimensional Heat Conduction" Problem

As shown in Fig. 2, this problem involves rectangular plates with a width of L and a height of W. The temperature on the top boundary is T_2, and the temperatures on the other boundaries are equal to T_1. The governing equation of the temperature distribution in the rectangular plate is:

$$(\nabla\cdot\nabla)T=0 \tag{11}$$

where $\nabla=[\partial/\partial x_1\ \ \partial/\partial x_2]^T$ is the del operator. This equation can be solved by using the finite volume method with boundary conditions. Thus, integrating Eq. (11) by the finite volume of a central cell obtains:

$$\int_{CV}\left((\nabla\cdot\nabla)T\right)d\forall=0 \tag{12}$$

Then, applying Gauss's divergence theorem to Eq. (12) obtains:

$$\int_{CS}\left((\mathbf{n}\cdot\nabla)T\right)dA=0 \tag{13}$$

Equation (13) can be expanded to:

$$\left(\frac{\partial T}{\partial x_1}d(x_2)_C\right)_e-\left(\frac{\partial T}{\partial x_1}d(x_2)_C\right)_w+\left(\frac{\partial T}{\partial x_2}d(x_1)_C\right)_n-\left(\frac{\partial T}{\partial x_2}d(x_1)_C\right)_s=0 \tag{14}$$

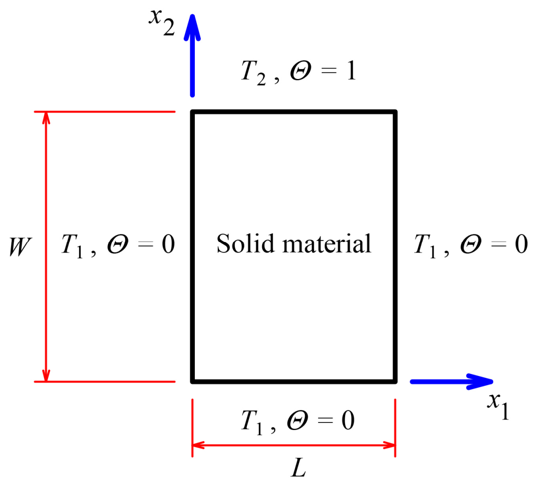

Fig. 2. Schematic of the "steady-state two-dimensional heat conduction" problem.

Table 4. Comparison of the VS-LIP solutions with the analytical solutions to the "steady-state two-dimensional heat conduction" problem.

x_2^{**}	Θ_A	Θ_N	
		6th Order accuracy (Error %)	12th Order accuracy (Error %)
0.1	0.00151865	0.00152253 (0.25532269)	0.00152262 (0.26143239)
0.2	0.00318842	0.00319645 (0.25194031)	0.00319663 (0.25760271)
0.3	0.00517545	0.00518605 (0.20487466)	0.00518631 (0.20984938)
0.4	0.00767745	0.00769376 (0.21244829)	0.00769408 (0.21663272)
0.5	0.01094333	0.01096427 (0.19130620)	0.01096464 (0.19470083)
0.6	0.01529793	0.01531770 (0.12922146)	0.01531811 (0.13189333)
0.7	0.02117416	0.02121026 (0.17047082)	0.02121069 (0.17252124)
0.8	0.02915571	0.02919128 (0.12202240)	0.02919173 (0.12356467)
0.9	0.04003410	0.04006541 (0.07821720)	0.04006587 (0.07935872)
1.0	0.05488490	0.05491792 (0.06016712)	0.05491838 (0.06100144)
1.1	0.07516809	0.07520658 (0.05120403)	0.07520703 (0.05180687)
1.2	0.10285655	0.10292689 (0.06837746)	0.10292733 (0.06880741)
1.3	0.14058969	0.14071016 (0.08568930)	0.14071058 (0.0859907)
1.4	0.19182936	0.19185984 (0.01589028)	0.19186024 (0.01609682)
1.5	0.26094334	0.26105147 (0.04144014)	0.26105183 (0.04157731)
1.6	0.35302698	0.35312705 (0.02834843)	0.35312736 (0.0284356)
1.7	0.47307767	0.47306512 (0.00265211)	0.47306537 (0.0026004)
1.8	0.62398050	0.62402636 (0.00734873)	0.62402653 (0.00737588)
1.9	0.80320814	0.80320683 (0.00016280)	0.80320692 (0.00015205)

The VS-LIP scheme is used to discretize the derivative values of the temperature with respect to time and space on the central cell and cell faces, respectively. Therefore, the temperature distribution on the rectangular plate can be derived as follows:

$$\sum_{na=1}^{2}\left(\sum_{nf=1}^{2}\left(\left((-1)^{nf}\,d(x_{nna})_{0,\,i(nna)}\right)\sum_{nc=1}^{ncmax(na)}\left(DLX_{na,\,nf,\,i(na),\,nc}T_{i1+ncc1,\,i2+ncc2}\right)\right)\Big|\text{Costraint-A}\right)=0$$

$$\text{Constraint-A}=\begin{cases}\text{If}\,(na=1)\,\text{then}\,(nna=2)\,\text{endif}\\ \text{If}\,(na=2)\,\text{then}\,(nna=1)\,\text{endif}\end{cases} \tag{15}$$

Equation (15) can be rearranged to obtain:

$$T_{i1,\,i2}=\frac{-\sum_{na=1}^{2}\left(\sum_{nf=1}^{2}\left(\left((-1)^{nf}\,d(x_{nna})_{0,\,i(nna)}\right)\sum_{nc=1}^{ncmax(na)}\left(DLX_{na,\,nf,\,i(na),nc}T_{i1+ncc1,\,i2+ncc2}\right)\right)\Big|\text{Constraint-B}\right)}{\sum_{na=1}^{2}\left(\sum_{nf=1}^{2}\left(\left((-1)^{nf}\,d(x_{nna})_{0,\,i(nna)}\right)\sum_{nc=1}^{ncmax(na)}\left(DLX_{na,\,nf,\,i(na),\,nc}\right)\right)\Big|\text{Constraint-C}\right)} \tag{16}$$

where

$$\text{Constraint-B}=\begin{cases}\text{If}\,(na=1)\,\text{then}\,(nna=2)\,\text{endif}\\ \text{If}\,(na=2)\,\text{then}\,(nna=1)\,\text{endif}\\ \text{When}\;ncc1\neq0\;\text{or}\;ncc2\neq0\end{cases}$$

$$\text{Constraint-C}=\begin{cases}\text{If}\,(na=1)\,\text{then}\,(nna=2)\,\text{endif}\\ \text{If}\,(na=2)\,\text{then}\,(nna=1)\,\text{endif}\\ \text{When}\;ncc1=0\;\text{and}\;ncc2=0\end{cases}$$

For assessment, the relative error value of the developed code is defined as 10^{-10}. The cell numbers used to determine solutions to the problem are set to 51×101. The code is run to compute the temperature distribution directly from the dimensional parameters, but the solutions are changed to be dimensionless. The dimensionless temperature is $\Theta=(T-T_1)/(T_2-T)$.

Table 4 compares the VS-LIP solutions (Θ_N) with the analytical solutions as [32]:

$$\left(\Theta_A(x_1,x_2)=\frac{2}{\pi}\sum_{n=1}^{\infty}\left(\frac{(-1)^{n+1}+1}{n}\sin\left(\frac{n\pi x_1}{L}\right)\frac{\sinh(n\pi x_2/L)}{\sinh(n\pi W/L)}\right)\right)\;\text{at}\;x_1^{**}=x_1/L=0.5\;\text{and}\;x_2^{**}=x_2/L$$

The relative percentage error can be computed from $\text{ERROR}\,\%=(|\,\Theta_A-\Theta_N\,|\times100)/\Theta_A$.

Figure 3 shows the dimensionless temperature contours in the rectangular plate of the VS-LIP solutions. The contour values and patterns are the same as those shown in [32].

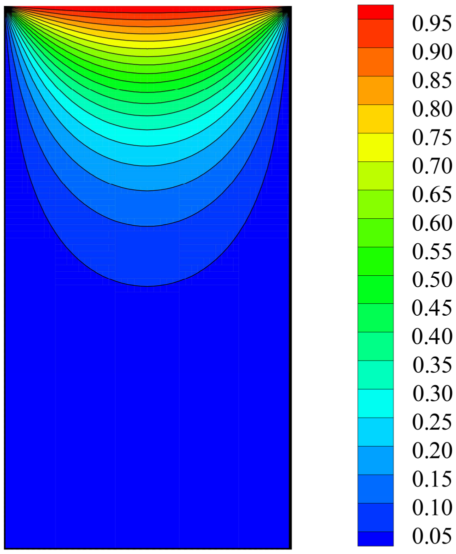

Fig. 3. Dimensionless temperature contours of the VS-LIP solutions to the “steady-state two-dimensional heat conduction” problem.

3.3. “One-Dimensional Burgers’ Equation” Problem

The one-dimensional Burgers’ equation is expressed as:

$$\frac{\partial u}{\partial t} + (u \cdot \nabla)u = \frac{1}{Re}(\nabla \cdot \nabla)u \tag{17}$$

where u, Re, and ∇ are the velocity, Reynolds number, and del operator $(\nabla = \partial / \partial x)$, respectively. Equation (17) can be solved by applying the finite volume method with the VS-LIP scheme:

$$u_{ntmax,\,i1} = \frac{\left(-\sum_{nt=1}^{ntmax-1} \left(DLT_{nt}\, u_{nt,\,i1} \right) d(x_1)_{0,\,i1} - \sum_{nf=1}^{2} \left((-1)^{nf} \begin{pmatrix} (u)_{nf,\,i1} \sum_{nc=1}^{ncmax} \left(LX_{1,\,nf,\,i1,\,nc} u_{ntmax,\,i1+ncc1} \right) \\ -\frac{1}{Re} \sum_{nc=1}^{ncmax} \left(DLX_{1,\,nf,\,i1,\,nc} u_{ntmax,\,i1+ncc1} \right) \end{pmatrix} \right) \Bigg| \text{When } ncc1 \neq 0 \right)}{\left(DLT_{ntmax}\, d(x_1)_{0,\,i1} + \sum_{nf=1}^{2} \left((-1)^{nf} \begin{pmatrix} (u)_{nf,\,i1} \sum_{nc=1}^{ncmax} \left(LX_{1,\,nf,\,i1,\,nc} \right) \\ -\frac{1}{Re} \sum_{nc=1}^{ncmax} \left(DLX_{1,\,nf,\,i1,\,nc} \right) \end{pmatrix} \right) \Bigg| \text{When } ncc1 = 0 \right)} \tag{18}$$

For this assessment, the initial and boundary conditions of Eq. (18) are given as $u(0,x) = (2/Re)(\pi \sin(\pi x))/(2+\cos(\pi x))$, $u(t,0) = u(t,1) = 0,\ x \in (0,1)$ The exact solution [23] is calculated from $u(t,x) = (2/Re)(\pi e^{-\pi^2 t/\mathrm{Re}} \sin(\pi x))/(2 + e^{-\pi^2 t/\mathrm{Re}} \cos(\pi x))$.

Table 5 compares the exact solution and VS-LIP solution. The total number of cells is 40. The time step is 0.0001, and the time to obtain the solution is 0.001. The relative residual error for numerical and exact solutions is 10^{-10} for this case.

3.4. “Lid-Driven Cavity Flow” and “Natural Convection in a Rectangular Cavity” Problems

Because the “lid-driven cavity flow” and “natural convection in a rectangular cavity” problems share some similar governing equations, they are presented together in this section. Figure 4 shows the “lid-driven cavity flow” problem, where a square cavity of width b is filled with an incompressible fluid. All velocity components of the fluid on the cavity walls are equal to zero except for the horizontal velocity on the top wall, which is $-U$. The gravitational acceleration is neglected in the computation. Fig. 5 shows the “natural convection in a rectangular cavity” problem, where air circulates in a rectangular cavity. The airflow can be defined by using the continuity, momentum, and energy equations. Because of the slow airflow in the cavity, the flow is assumed incompressible except for the density in the body force term in the momentum equation in the vertical direction. A no-slip condition is applied to the air velocity on the cavity walls. The cavity has a width b and height h. The hot and cold temperatures on the left and right walls of the cavity are denoted by T_{hot} and T_{cold}, respectively. The bottom and top walls of the cavity are adiabatic.

The governing equations defining fluid flow in a cavity for the two-dimensional problems can be written as:

$$\nabla \cdot \mathbf{V} = 0 \tag{19}$$

$$\alpha \frac{\partial \Phi}{\partial t} + \alpha(\mathbf{V} \cdot \nabla)\Phi = \Gamma(\nabla \cdot \nabla)\Phi + \mathbf{S}_{\Phi} \tag{20}$$

Table 6 defines the variables in Eqs. (19) and (20).

For the “natural convection in a rectangular cavity” problem, the Boussinesq approximation can be adopted for the compressible air density in the body force term. The VS-LIP scheme can be used with the finite volume method to solve Eq. (20). Then, the values of the variables can be computed.

Table 7 defines the variables in Eq. (21).

Table 5. Comparison of solutions to the one-dimensional Burgers' equation problem.

Re	Spatial location	Exact solution	Present work	
			6^{th} Order accuracy (Error %)	12^{th} Order accuracy (Error %)
2	0.1	0.3278695754	0.3267946846 (0.3278409711)	0.3267946846 (0.3278409711)
	0.2	0.6550692681	0.6529285016 (0.3268000201)	0.6529285015 (0.3268000273)
	0.3	0.9784125669	0.9752677868 (0.3214165687)	0.9752677867 (0.3214165837)
	0.4	1.2884635831	1.2844134070 (0.3143415268)	1.284413407 (0.3143415283)
	0.5	1.5630639473	1.5585969563 (0.2857842769)	1.5585969572 (0.2857842227)
	0.6	1.7566421900	1.7531995530 (0.1959782715)	1.7531995569 (0.1959780525)
	0.7	1.7872064195	1.7878429538 (0.0356161601)	1.7878429582 (0.0356164049)
	0.8	1.5376942857	1.5429825430 (0.3439082365)	1.5429825301 (0.3439073991)
	0.9	0.9168595149	0.9216850733 (0.5263138269)	0.9216850490 (0.5263111772)
10	0.1	0.0657497637	0.0657059372 (0.0666565110)	0.0657059372 (0.0666565110)
	0.2	0.1313829447	0.1312947974 (0.0670918781)	0.1312947974 (0.0670918781)
	0.3	0.1962808815	0.1961483323 (0.0675303560)	0.1961483323 (0.0675303560)
	0.4	0.2585757552	0.2583746199 (0.0777858366)	0.2583746199 (0.0777858366)
	0.5	0.3138493748	0.3135611167 (0.0918459968)	0.3135611167 (0.0918459968)
	0.6	0.3529718374	0.3526424603 (0.0933154101)	0.3526424604 (0.0933153652)
	0.7	0.3594428643	0.3593238624 (0.0331073224)	0.3593238626 (0.0331072727)
	0.8	0.3095803641	0.3096052036 (0.0080236303)	0.3096052031 (0.0080234518)
	0.9	0.1847536857	0.1845688979 (0.1000184660)	0.1845688975 (0.1000186914)
100	0.1	0.0065789364	0.0065784438 (0.0074877719)	0.0065784438 (0.0074877719)
	0.2	0.0131466076	0.0131455270 (0.0082191044)	0.0131455270 (0.0082191044)
	0.3	0.0196415692	0.0196396223 (0.0099125009)	0.0196396223 (0.0099125009)
	0.4	0.0258774791	0.0258712649 (0.0240139742)	0.0258712649 (0.0240139742)
	0.5	0.0314128280	0.0313978537 (0.0476694619)	0.0313978537 (0.0476694619)
	0.6	0.0353342824	0.0353095931 (0.0698734434)	0.0353095931 (0.0698734434)
	0.7	0.0359895216	0.0359719463 (0.0488346241)	0.0359719463 (0.0488346241)
	0.8	0.0310042324	0.0309828455 (0.0689805669)	0.0309828455 (0.0689805669)
	0.9	0.0185066702	0.0184615697 (0.2436989440)	0.0184615697 (0.2436989440)
500	0.1	0.0013158577	0.0013158285 (0.0022211546)	0.0013158285 (0.0022211546)
	0.2	0.0026294693	0.0026293910 (0.0029781422)	0.0026293910 (0.0029781422)
	0.3	0.0039285536	0.0039283657 (0.0047820920)	0.0039283657 (0.0047820920)
	0.4	0.0051758498	0.0051748548 (0.0192244580)	0.0051748548 (0.0192244580)
	0.5	0.0062830617	0.0062803139 (0.0437329558)	0.0062803139 (0.0437329558)
	0.6	0.0070675164	0.0070627258 (0.0677835382)	0.0070627258 (0.0677835382)
	0.7	0.0071987092	0.0071950928 (0.0502373500)	0.0071950928 (0.0502373500)
	0.8	0.0062016687	0.0061969646 (0.0758511075)	0.0061969646 (0.0758511075)
	0.9	0.0037018913	0.0036923952 (0.2565200572)	0.0036923952 (0.2565200572)

Table 6. Details of variables in Eqs. (19) and (20).

Problem	Vectors of Eqs. (19) and (20)	Variables in the momentum equation in the horizontal direction of Eq. (20)	Variables in the momentum equation in the vertical direction of Eq. (20)	Variables in the energy equation of Eq. (20)
"Lid-driven cavity flow"	$\mathbf{V}=[u \quad v]^T$, $\Phi=[u \quad v]^T$, and $\mathbf{S}_\Phi=[S_u \quad S_v]^T$	$\alpha=\rho$, $\Gamma=\mu$, and $S_u=-\dfrac{\partial p}{\partial x_1}$	$\alpha=\rho$, $\Gamma=\mu$, and $S_v=-\dfrac{\partial p}{\partial x_2}$	-
"Natural convection in a square cavity"	$\mathbf{V}=[u \quad v]^T$, $\Phi=[u \quad v \quad T]^T$, and $\mathbf{S}_\Phi=[S_u \quad S_v \quad S_T]^T$	$\alpha=\rho$, $\Gamma=\mu$, and $S_u=-\dfrac{\partial p}{\partial x_1}$	$\alpha=\rho$, $\Gamma=\mu$, and $S_v=-\dfrac{\partial p}{\partial x_2}-\rho_{i,j}g$	$\alpha=\rho c_p$, $\Gamma=k$, and $S_T=0$

Note:

$\rho_{i,j}$: compressible density of air filled in the cavity. The density is defined by the Boussinesq approximation, which can be calculated from $\rho_{i,j}=\rho_0(1-\beta(T_{i,j}-T_0))$.

T_0: reference temperature computed from $T_0=(T_{hot}+T_{cold})/2$.

β: volumetric thermal expansion coefficient obtained from $\beta=1/T_0$.

ρ_0: density of air at the reference temperature. u and v: velocity components in the horizontal and vertical directions, respectively.

p: static pressure.

μ, k, c_p: viscosity, thermal conductivity, and specific heat at the constant pressure, respectively.

g: gravitational acceleration.

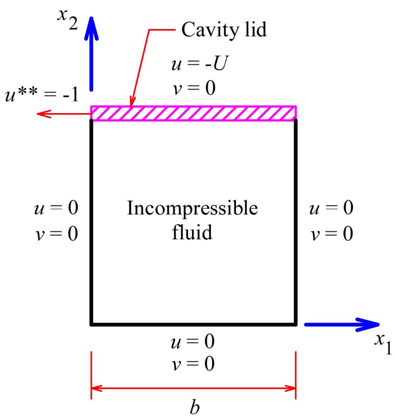

Fig. 4. Schematic of the "lid-driven cavity flow" problem.

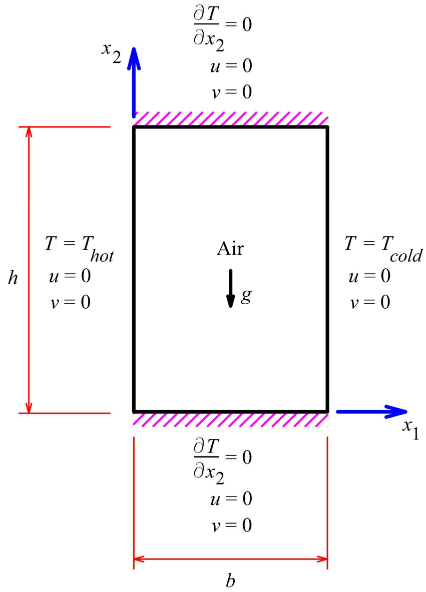

Fig. 5. Schematic of the "natural convection in a rectangular cavity" problem.

$$\phi_{ntmax,i1,i2} = \frac{\left(\begin{matrix} \left(S_\phi - \alpha \sum_{nt=1}^{ntmax-1} \left(DLT_{nt}\, \phi_{nt,i1,i2}\right)\right)\left(d(x_1)_{0,i1}\, d(x_2)_{0,i2}\right) \\ -\sum_{na=1}^{2} \left(d(x_{nna})_{0,i(nna)} \sum_{nf=1}^{2} \left(\left((-1)^{nf}\right) \left(\sum_{nc=1}^{ncmax(na)} \left(\begin{matrix} \alpha (V_{na})_{nf,i1,i2}\, LX_{na,nf,i(na),nc} \\ -\Gamma\, DLX_{na,nf,i(na),nc} \end{matrix} \right) \phi_{ntmax,i1+ncc1,i2+ncc2} \right) \Big| \text{Constraint-B} \right)\right) \end{matrix}\right)}{\left(\begin{matrix} \alpha\, DLT_{ntmax}\left(d(x_1)_{0,i1}\, d(x_2)_{0,i2}\right) \\ +\sum_{na=1}^{2} \left(d(x_{nna})_{0,i(nna)} \sum_{nf=1}^{2} \left(\left((-1)^{nf}\right) \left(\sum_{nc=1}^{ncmax(na)} \left(\begin{matrix} \alpha (V_{na})_{nf,i1,i2}\, LX_{na,nf,i(na),nc} \\ -\Gamma\, DLX_{na,nf,i(na),nc} \end{matrix} \right) \Big| \text{Constraint-C} \right)\right)\right) \end{matrix}\right)} \tag{21}$$

The corrected pressure can be calculated by using the SIMPLE algorithm:

$$p'_{i1,i2} = \frac{\left(\left(\sum_{na=1}^{2}\left(\sum_{nf=1}^{2}\left(\begin{matrix}\left((-1)^{nf}\, d(x_{nna})_{0,i(nna)}\right) \\ \sum_{nc=1}^{ncmax(na)} \left(LX_{na,nf,i(na),nc} \left((V^*_{na})_{ip1,ip2} - \left(\begin{matrix} \left(\frac{d(x_1)_{0,ip1}\, d(x_2)_{0,ip2}}{(a_{na})_{ip1,ip2}}\right) \\ \sum_{ncp=1}^{ncmax(na)} \left(\begin{matrix} DLX_{na,nf,ip(na),ncp} \\ p'_{ip1+nccp1,ip2+nccp2} \end{matrix} \right) \end{matrix} \right) \Big| \text{Constraint-D} \right)\right)\end{matrix}\right)\right) \Big| \text{Constraint-A} \right)\right)}{\left(\sum_{na=1}^{2}\left(\sum_{nf=1}^{2}\left(\begin{matrix}\left((-1)^{nf}\, d(x_{nna})_{0,i(nna)}\right) \\ \sum_{nc=1}^{ncmax(na)} \left(LX_{na,nf,i(na),nc} \left(\begin{matrix} \left(\frac{d(x_1)_{0,ip1}\, d(x_2)_{0,ip2}}{(a_{na})_{ip1,ip2}}\right) \\ \sum_{ncp=1}^{ncmax(na)} \left(DLX_{na,nf,ip(na),ncp} \right) \end{matrix} \right) \Big| \text{Constraint-E} \right)\end{matrix}\right)\right) \Big| \text{Constraint-A} \right)} \tag{22}$$

where

$$(V^*_1)_{ip1,ip2} = (u^*)_{ip1,ip2}\,,\; (V^*_2)_{ip1,ip2} = (v^*)_{ip1,ip2}\,,$$

$$\text{Constraint-D} = \begin{cases} \text{When } (ip1 + nccp1 \neq i1) \\ \text{or } (ip2 + nccp2 \neq i2) \end{cases},\; \text{Constraint-E} = \begin{cases} \text{When } (ip1 + nccp1 = i1) \\ \text{and } (ip2 + nccp2 = i2) \end{cases}$$

$$ip(na) = i(na) + ncc(na)\,,$$

$$nccp(na) = ncp - nch(na, nf, ip(na))\,,$$

$$(a_{na})_{ip1,ip2} = \left(\begin{matrix} \rho\, DLT_{ntmax}\left(d(x_1)_{0,ip1}\, d(x_2)_{0,ip2}\right) \\ +\sum_{na=1}^{2}\left(\sum_{nf=1}^{2}\left(\left((-1)^{nf}\; d(x_{nna})_{0,ip(nna)}\right) \sum_{nc=1}^{ncmax(na)} \left(\begin{matrix} \rho (V_{na})_{nf,ip1,ip2}\, LX_{na,nf,ip(na),nc} \\ -\mu DLX_{na,nf,ip(na),nc} \end{matrix} \right) \Big| \text{Constraint-C} \right)\right) \end{matrix}\right)$$

Table 7. Details of variables in Eq. (21).

Problem	Variables in the momentum equation in the horizontal direction of Eq. (21)	Variables in the momentum equation in the vertical direction of Eq. (21)	Variables in the energy equation of Eq. (21)
"Lid-driven cavity flow"	$\phi_{ntmax,i1,i2} = u^{*}_{i1,i2}$, $\phi_{nt,i1,i2} = u_{nt,i1,i2}$, $(V_1)_{nf,i1,i2} = (u)_{nf,i1,i2}$, $(V_2)_{nf,i1,i2} = (v)_{nf,i1,i2}$, and $S_\phi = -\sum_{nc=1}^{ncmax(1)} \left(DLX_{1,0,i1,nc}\, p_{i1+ncc1,i2+ncc2} \right)$	$\phi_{ntmax,i1,i2} = u^{*}_{i1,i2}$, $\phi_{nt,i1,i2} = u_{nt,i1,i2}$, $(V_1)_{nf,i1,i2} = (u)_{nf,i1,i2}$, $(V_2)_{nf,i1,i2} = (v)_{nf,i1,i2}$, and $S_\phi = -\sum_{nc=1}^{ncmax(2)} \left(DLX_{2,0,i2,nc}\, p_{i1+ncc1,i2+ncc1} \right)$	-
"Natural convection in a square cavity"	$\phi_{ntmax,i1,i2} = u^{*}_{i1,i2}$, $\phi_{nt,i1,i2} = u_{nt,i1,i2}$, $(V_1)_{nf,i1,i2} = (u)_{nf,i1,i2}$, $(V_2)_{nf,i1,i2} = (v)_{nf,i1,i2}$, and $S_\phi = -\sum_{nc=1}^{ncmax(1)} \left(DLX_{1,0,i1,nc}\, p_{i1+ncc1,i2+ncc2} \right)$	$\phi_{ntmax,i1,i2} = u^{*}_{i1,i2}$, $\phi_{nt,i1,i2} = u_{nt,i1,i2}$, $(V_1)_{nf,i1,i2} = (u)_{nf,i1,i2}$, $(V_2)_{nf,i1,i2} = (v)_{nf,i1,i2}$, and $S_\phi = \begin{pmatrix} -\sum_{nc=1}^{ncmax(2)} \left(DLX_{2,0,i2,nc}\, p_{i1+ncc1,i2+ncc2} \right) \\ -\rho_{i,j} g \end{pmatrix}$	$\phi_{ntmax,i1,i2} = T_{ntmax,i1,i2}$, $\phi_{nt,i1,i2} = T_{nt,i1,i2}$, $(V_1)_{nf,i1,i2} = (u)_{nf,i1,i2}$, $(V_2)_{nf,i1,i2} = (v)_{nf,i1,i2}$, and $S_\phi = 0$

Table 8. Comparison of the VS-LIP solutions with the benchmark and published numerical solutions to the "lid-driven cavity flow" problem at Re = 1000, where the solution values lie on the horizontal centerline of the square cavity.

x_1^{**}	p^{**}			ω		
	Present work	[33]	[34]	Present work	[33]	[34]
0.0000	0.077036	0.077455	0.077429	-5.33857	-5.462170	-5.49670
0.0312	0.078017	0.078837		-8.40592	-8.443500	
0.0391	0.077348	0.078685	0.078658	-8.23632	-8.246160	-8.24620
0.0469	0.077362	0.087148		-7.59021	-7.585240	
0.0547	0.075855	0.077154	0.077128	-6.51647	-6.508670	-6.50970
0.0937	0.065024	0.065816		0.89892	0.92291	
0.1406	0.048291	0.049029	0.049004	3.39638	3.43016	3.42940
0.1953	0.034115	0.034552		2.21513	2.21171	
0.5000	0.000000	0.000000	0.000000	2.05870	2.06722	2.06690
0.7656	0.044515	0.044848		2.04662	2.06122	
0.7734	0.046585	0.047260	0.047259	1.98610	2.00174	2.00100
0.8437	0.068828	0.069511		0.73014	0.74207	
0.9062	0.083210	0.084386	0.084369	-0.81818	-0.823980	-0.82517
0.9219	0.085531	0.086716		-1.23152	-1.239910	
0.9297	0.086585	0.087653	0.087625	-1.49309	-1.503060	-1.50250
0.9375	0.087301	0.088445		-1.82126	-1.833080	
1.0000	0.089235	0.090477	0.090448	-7.59419	-7.663690	-7.63330

Table 9. Comparison of the VS-LIP solutions with the benchmark and published numerical solutions to the "lid-driven cavity flow" problem at Re = 1000, where the solution values lie on the vertical centerline of the square cavity.

x_1^{**}	p^{**}			ω		
	Present work	[33]	[34]	Present work	[33]	[34]
1.0000	0.052662	0.052987	0.052971	15.00001	14.75340	14.7920
0.9766	0.050956	0.052009		12.06494	12.06700	
0.9688	0.050112	0.051514	0.051493	9.47013	9.49496	9.4781
0.9609	0.049837	0.050949		6.93754	6.95968	
0.9531	0.049054	0.050329	0.050314	4.84723	4.85754	4.8628
0.8516	0.034250	0.034910		1.75024	1.76200	
0.7344	0.011847	0.012122	0.012113	2.08288	2.09121	2.0909
0.6172	-0.000651	-0.0008270		2.05717	2.06539	
0.5000	0.000000	0.000000	0.000000	2.05870	2.06722	2.0669
0.4531	0.004353	0.004434		2.05345	2.06215	
0.2813	0.040523	0.040377	0.040381	2.26183	2.26772	2.2678
0.1719	0.081126	0.081925		1.02554	1.05467	
0.1016	0.103279	0.104187	0.104416	-1.61957	-1.63436	-1.6352
0.0703	0.107926	0.108566		-2.17839	-2.20175	
0.0625	0.107937	0.109200	0.109160	-2.29373	-2.31786	-2.3174
0.0547	0.109028	0.109689		-2.42455	-2.44960	
0.0000	0.109092	0.110591	0.110560	-4.12620	-4.16648	-4.1554

The corrected velocity components can then be obtained from:

$$(V_{na})_{ntmax,\,i1,\,i2} = (V^{*}_{na})_{i1,\,i2} - \left(\left(\frac{d(x_1)_{0,\,i1}\, d(x_2)_{0,\,i2}}{(a_{na})_{i1,\,i2}}\right)\sum_{nc=1}^{ncmax(na)}\left(DLX_{na,\,nf,\,i(na),\,nc}\; p'_{i1+ncc1,\,i2+ncc2}\right)\right) \tag{23}$$

where $(V_1)_{ntmax,\,i1,\,i2} = u_{ntmax,\,i1,\,i2}$ and $(V_2)_{ntmax,\,i1,\,i2} = v_{ntmax,\,i1,\,i2}$.

Finally, the corrected pressure can be computed from:

$$p_{i1,\,i2} = p^{*}_{i1,\,i2} + p'_{i1,\,i2} \tag{24}$$

The VS-LIP solutions are compared against the benchmark, published, and experimental solutions to the “lid-driven cavity flow” and “natural convection in a rectangular cavity” problems [30, 33-50] for assessment. The VS-LIP solutions (present work) use time steps and order of accuracy of *ntmax* = 4, and *ncmax*(1) and *ncmax*(2) equal to 6, respectively. The dimensionless time step ($\Delta t^{**} = \Delta t|U|/b$ for the “lid-driven cavity flow” problem and $\Delta t^{**} = \Delta t\sqrt{g\beta(T_{hot} - T_{cold})/b}$ for the “natural convection in a rectangular cavity” problem) is set to 0.001 to run the code. The relative error values of the developed codes are 10^{-5} and 10^{-4} for the “lid-driven cavity flow” and “natural convection in a rectangular cavity” problems, respectively. The cell numbers of the simulations for the “lid-driven cavity flow” problem at the Reynolds numbers (*Re*s) of 1000 and 5000 are 100 × 100 and 160 × 160, respectively. The “natural convection in a rectangular cavity” problem can be divided into two problems: natural convection in a square cavity and natural convection in a tall cavity. The cell numbers of the simulations for the “natural convection in a square cavity” problem is 80 × 80 for Rayleigh numbers (*Ra*s) of 10^5 and 10^6 and then 160 × 160 for *Ra*s of 10^7 and 10^8. The cell numbers of the simulation for the “natural convection in a tall cavity” problem is 80 × 400 for *Ra* of 1.1×10^4, and the aspect ratio (*AR*) is equal to 16. Non-uniform grids are employed for the simulations. The fine grids are located near the cavity walls, and the coarse grids are assigned to the core area of the cavities. The ratios of the gap sizes between the coarse grid to the consecutive fine grid are 1.01 for both the horizontal and vertical axes of the “lid-driven cavity flow” and “natural convection in a square cavity” problem. They are 1.01 and 1.00 for the horizontal and vertical axes of the “natural convection in a tall cavity” problem, respectively.

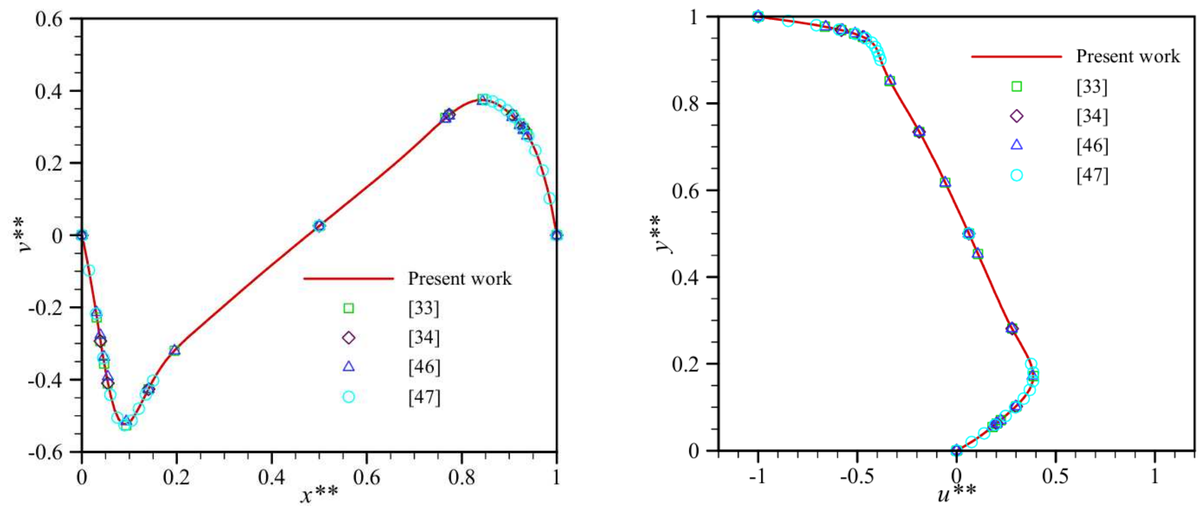

(a) (b)

Fig. 6. Velocity profile of fluid flow in the “lid-driven cavity flow” problem at *Re* = 1000: (a) along the horizontal centerline and (b) along the vertical centerline.

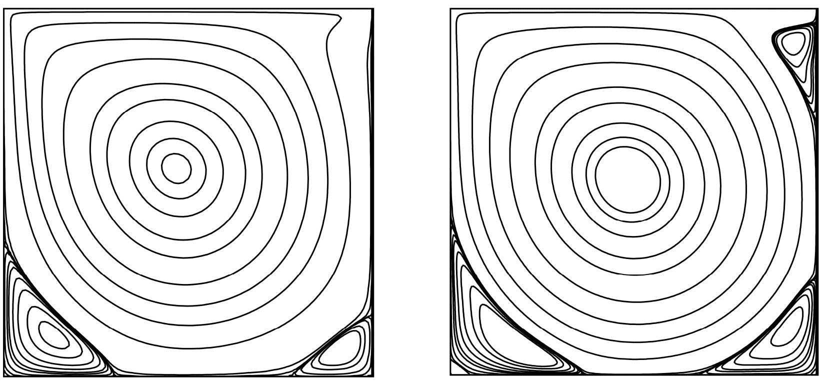

(a) (b)

Fig. 7. Streamline and vorticity contours of the VS-LIP solutions to the “lid-driven cavity flow” problem: (a) streamline contour at *Re* = 1000, (b) streamline contour at *Re* = 5000, (c) vorticity contour at *Re* = 1000, and (d) vorticity contour at *Re* = 5000.

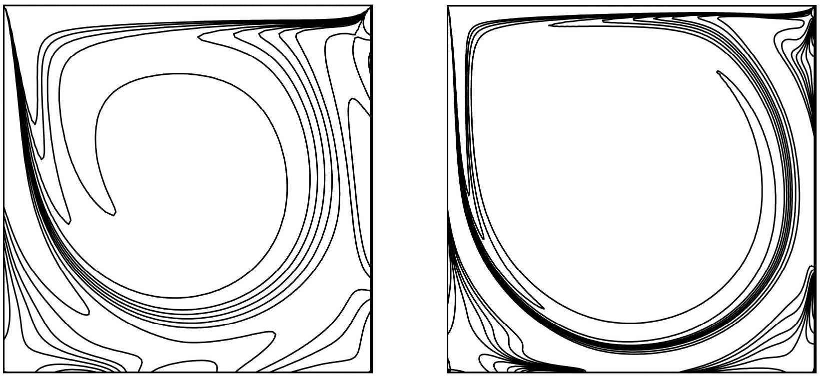

(c) (d)

Fig. 7. continued.

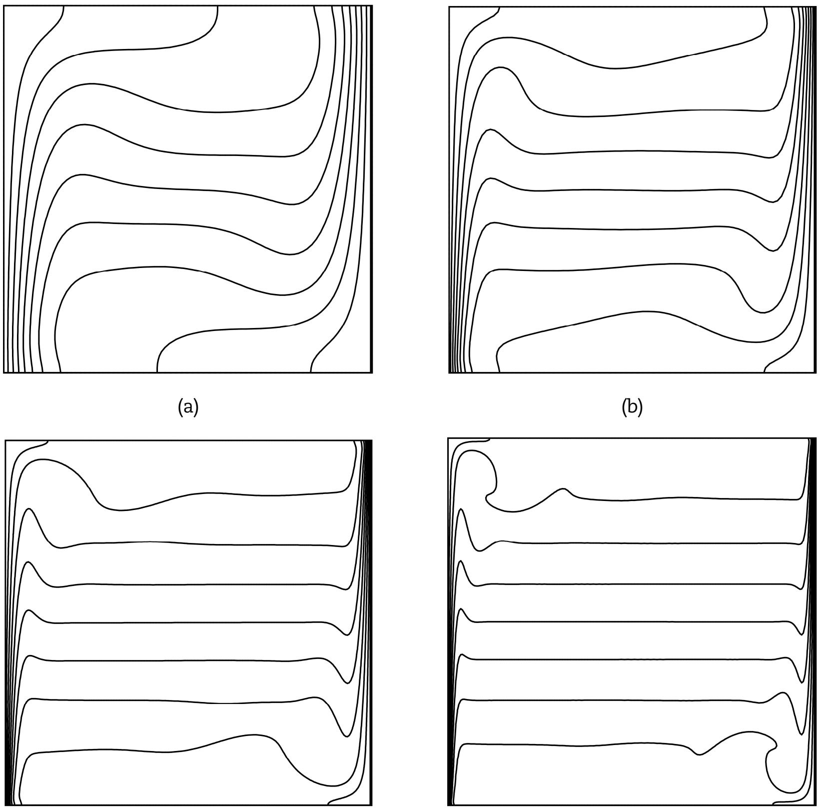

(a) (b)

(c) (d)

Fig. 8. Dimensionless temperature contours of the VS-LIP solutions to the "natural convection in a square cavity" problem: (a) Ra = 10^5, (b) Ra = 10^6, (c) Ra = 10^7, and (d) Ra = 10^8.

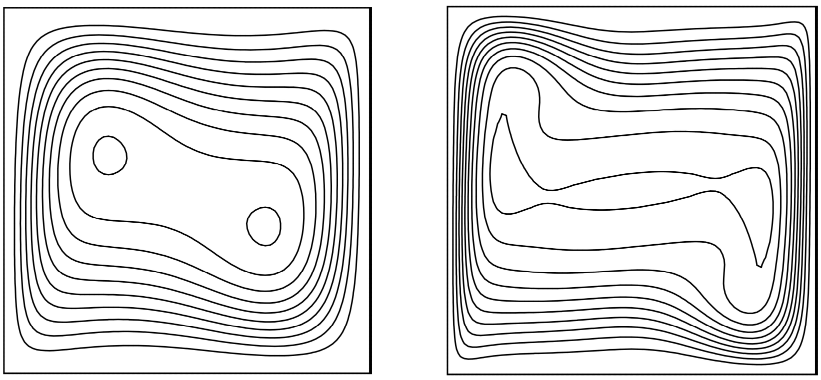

(a) (b)

Fig. 9. Streamline contours of the VS-LIP solutions to the "natural convection in a square cavity" problem: (a) Ra = 10^5, (b) Ra = 10^6, (c) Ra = 10^7, and (d) Ra = 10^8.

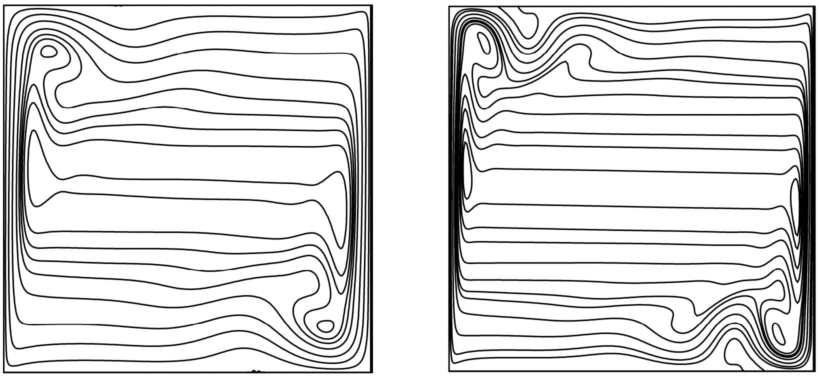

(c) (d)

Fig. 9. Continued.

Tables 8 and 9 compare the VS-LIP solutions with the benchmark and published numerical solutions of the “lid-driven cavity flow” problem at *Re* equals 1000. The solution values lay on the vertical and horizontal centerlines of the square cavity. The dimensionless parameters in Tables 8 and 9 can be computed from $x_1^{**} = x_1/b$, $x_2^{**} = x_2/b$, $p^{**} = p/\rho U^2$, and the vorticity $\omega = dv^{**}/dx_1^{**} - du^{**}/dx_2^{**}$. The VS-LIP solutions and solutions in [33, 34] are nearly the same.

Table 10 compares the VS-LIP solutions with the published solutions in [34] for the primary vortex and lower-left secondary vortex at *Re* = 5000. The solutions for the primary vortex comprise the maximum value of the streamline, vorticity, and corresponding dimensionless coordinate. The solutions for the lower-left secondary vortex comprise the minimum value of the streamline, the vorticity, and the corresponding dimensionless coordinate.

Figure 6 displays the dimensionless velocity profiles of fluid flow in the “lid-driven cavity flow” problem at *Re* = 1000 along the horizontal and vertical centerlines of the cavity. The dimensionless velocity components in the horizontal and vertical directions can be calculated from $u^{**} = u/U$ and $v^{**} = v/U$, respectively. Both dimensionless velocity profiles are compared with benchmark and published data [33, 34, 46, 47]. The profile lines are drawn at the same locations of the data coordinates.

Figure 7 shows the streamline (ψ) and vorticity contours of the flow in the square cavity, which are computed by using the VS-LIP scheme at *Re* = 1000 and *Re* = 5000. The streamline can be received from $(\nabla \cdot \nabla)\psi = -\omega.$ The contour values displayed in Fig. 7 are rearranged according to the contour values in [33]. Figures 7(a) and (c) are similar to the results in [33], and Figs. 7(b) and (d) are similar to the results in [34].

Table 11 presents the average Nusselt numbers and dimensionless maximum velocities in the horizontal and vertical directions on the vertical and horizontal centerlines of the square cavity. The average Nusselt numbers [30] can be computed from $\overline{Nu} = (1/b)\int_0^b ((q''|_{x_1=0} + q''|_{x_1=b})/2q''_{ref})dx_2$, $q'' = k(dT/dx_1)$, and $q''_{ref} = k(T_{hot} - T_{cold})/b$. The maximum dimensionless velocities in the horizontal and vertical directions can be calculated from $u^{**}_{max} = u_{max}(\rho c_p b)/k$ and $v^{**}_{max} = v_{max}(\rho c_p b)/k$, respectively. The VS-LIP solutions are consistent with the benchmark and published numerical solutions.

Figures 8 and 9 show the dimensionless temperature and streamline contours of the airflow in the square cavity that are computed by using the VS-LIP scheme. The dimensionless temperature can be obtained from $T^{**} = (T - T_{cold})/(T_{hot} - T_{cold})$. The contour values in Figs. 8 and 9 conform to those in [35] for *Ra* = 10^5–10^6. Then Figs. 8 and 9 are similar to the results in [38] for *Ra* = 10^7–10^8.

Table 12 compares the average Nusselt numbers computed by using the VS-LIP scheme with the published experimental and numerical Nusselt numbers for the “natural convection in a tall cavity” problem at *Ra* = 1.1 × 10^4. The average Nusselt numbers computed from the VS-LIP scheme are nearly the same as the average of the published Nusselt numbers.

Figure 10 shows the dimensionless temperature and streamline contours of the VS-LIP solutions to the “natural convection in a tall cavity” problem at *Ra* = 1.1 × 10^4. The contour patterns are similar to those in [44].

4. Conclusion

This paper presented the VS-LIP scheme, which is the extension of the original LIP scheme that adopts a numerical notation instead of a letter notation to refer to computational cells in discrete equations. The VS-LIP scheme can be used to easily extend the order of accuracy. It is suitable for use with the finite volume method and rectangular cells on Cartesian coordinates. The VS-LIP scheme was assessed by comparing its solutions with analytical, benchmark, published, and experimental solutions to five classical problems. The comparison showed that the VS-LIP solutions agree very well with the analytical, benchmark, published, and experimental solutions.

Table 10. Comparison of the VS-LIP solutions with the published solutions on the primary vortex and the lower-left secondary vortex at *Re* = 5000.

Vortex	Solution	Present work	[34]
Primary vortex	$\psi_{\max}$	0.12129	0.12193
	ω	1.9256	1.9322
	x^{**}	0.48197	0.48535
	y^{**}	0.53569	0.53516
Lower-left secondary vortex	$\psi_{\min}$	-0.0031023	-0.0030694
	ω	-2.6681	-2.7245
	x^{**}	0.19358	0.19434
	y^{**}	0.73996	0.07324

Table 11. Comparison of the VS-LIP solutions with the benchmark and published numerical solutions to the “natural convection in a square cavity” problem.

Ra	Reference	$\overline{Nu}$	$u^{**}_{max}(X^{**}_2)$	$v^{**}_{max}(X^{**}_1)$
	Present work	4.5247	34.6974 (0.8506)	68.4524 (0.0693)
	[35]	4.5190	34.73 (0.855)	68.59 (0.066)
	[36]	4.4300	35.73 (0.857)	69.08 (0.067)
	[39]	4.5100	-	-
	[40]	4.5460	35.521 (0.8554)	68.655 (0.0664)
10^5	[41]	4.2280	-	-
	[30]	4.4230	-	-
	[42]	4.5218	34.7223	68.5094
	[48]	4.5217	34.8366 (0.8556)	68.5731 (0.0671)
	[49]	4.5255	34.7758 (0.8555)	68.7176 (0.06641)
	[50]	4.410	35.576 (0.856)	69.241 (0.064)
	Present work	8.8445	64.6650 (0.8506)	219.7511 (0.0368)
	[35]	8.8000	64.63 (0.850)	219.36 (0.0379)
	[37]	8.7126	64.389 (0.8512)	216.76 (0.03943)
	[36]	8.7540	68.81 (0.872)	221.8 (0.0135)
	[38]	8.8170	-	-
	[39]	8.8060	-	-
10^6	[40]	8.6520	64.186 (0.8496)	219.866 (0.0371)
	[41]	8.2430	-	-
	[30]	8.8560	-	-
	[42]	8.8267	64.7889	220.3715
	[48]	8.8016	64.9035 (0.8484)	218.853 (0.0407)
	[49]	8.8141	64.7115 (0.8516)	220.5469 (0.03906)
	[50]	8.679	67.027 (0.852)	227.712 (0.035)
	Present work	16.5440	148.2745 (0.8802)	694.0374 (0.0233)
	[38]	16.5230	-	-
	[40]	16.7900	164.236 (0.851)	701.922 (0.020)
10^7	[41]	16.0730	-	-
	[42]	16.5371	148.2929	698.8831
	[48]	16.641	149.529 (0.8860)	702.582 (0.0213)
	[49]	16.4598	147.0795 (0.8836)	700.9533 (0.0202)
	Present work	30.3275	321.7384 (0.9260)	2181.9965 (0.0104)
	[36]	32.0450	514.3 (0.941)	1812 (0.0135)
	[38]	30.2250	-	-
	[39]	30.1	-	-
10^8	[40]	30.5060	389.877 (0.937)	2241.374 (0.0112)
	[41]	31.339	-	-
	[42]	30.2787	316.8832	2224.25
	[48]	30.827	328.734 (0.940)	2250.628 (0.0121)
	[49]	30.0264	328.2408 (0.9321)	2233.1374 (0.0122)

Table 12. Comparison of the average Nusselt numbers computed by using the VS-LIP scheme with the published experimental and numerical solutions to the “natural convection in a tall cavity” problem at $Ra = 1.1 \times 10^4$.

Reference	$\overline{Nu}$	Implementation
Present work	1.5236	Numerical
[43]	1.4307	Experimental
[44]	1.5250	Numerical
[45]	1.5351	Numerical

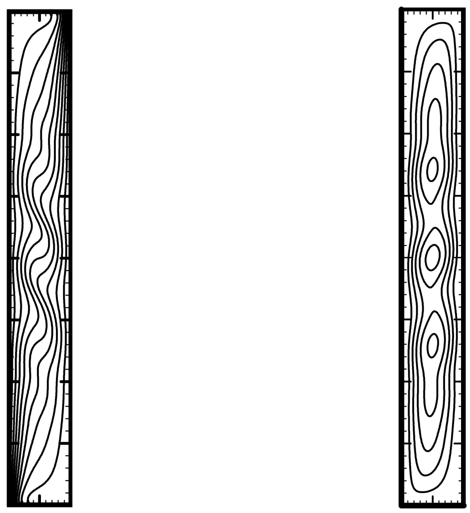

(a) (b)

Fig. 10. Dimensionless temperature and streamline contours of the VS-LIP solutions to the “natural convection in a tall cavity” problem at $Ra = 1.1 \times 10^4$: (a) temperature contour and (b) streamline contour.

Author Contributions

U. Prasopchingchana initiated the project, reviewed the literature, developed the mathematical modeling, examined the theory validation, developed the in-house codes, verified the codes, wrote the manuscript, and approved the final version of the manuscript.

Acknowledgment

The author wishes to acknowledge the National e-Science Infrastructure Consortium for providing computing resources contributing to the research results reported in this paper.

Conflict of Interest

The author declared no potential conflicts of interest concerning the research, authorship, and publication of this article.

Funding

The author received no financial support for the research, authorship, and publication of this article.

Data Availability Statement

The datasets generated and/or analyzed during the current study are available from the corresponding author upon reasonable request.

Appendix A

The constraints for calculation $nch\left(na,nf,i\left(na\right)\right)$ are as follows:

```
do na=1, 2
    do nf=0, 2
        if(nf=0)then
            do i=icmin(na),icmax(na)
                if(i=icmin(na))then
                nch(na,nf,i)=1
                else
                    if(i=icmax(na))then
                    nch(na,nf,i)=ncmax(na)
                    else
                        if((i-icmin(na)+1)<=((ncmax(na)/2)+1))then
                        nch(na,nf,i)=i-icmin(na)+1
                        else
                            if((icmax(na)-i+1)<=((ncmax(na)/2)+1))then
                            nch(na,nf,i)=ncmax(na)-(icmax(na)-i+1)+2
                            else
                            nch(na,nf,i)=(ncmax(na)/2)+1
                            end if
                        end if
                    end if
                end if
            end do
        else
            if(nf=1)then
                do i=icmin(na),icmax(na)
                    if((i-icmin(na)+1)<=((ncmax(na)/2)+1))then
                    nch(na,nf,i)=i-icmin(na)+1
                    else
                        if((icmax(na)-i+1),=(ncmax(na)/2))then
                        nch(na,nf,i)=ncmax(na)-(icmax(na)-i+1)+1
                        else
                        nch(na,nf,i)=(ncmax(na)/2)+1
                        end if
                    end if
                end do
            else
                do i=icmin(na),icmax(na)
                    if((i-icmin(na)+1)<=(ncmax(na)/2))then
                    nch(na,nf,i)=i-icmin(na)+1
                    else
                        if((icmax(na)-i+1)<=((ncmax(na)/2)+1))then
                        nch(na,nf,i)=ncmax(na)-(icmax(na)-i+1)+1
                        else
                        nch(na,nf,i)=ncmax(na)/2
                        end if
                    end if
                end do
            end if
        end if
    end do
end do
```

where $icmin(na)$ and $icmax(na)$ are the minimum and maximum numbers, respectively of the spatial grids on the na axis. The constraints start with how to compute $nch(na,nf,i(na))$ near the cavity walls, and then the value of $nch(na,nf,i(na))$ in the core cavity region is computed.

References

[1] Gerolymos, G. A., Sénéchal, D., Vallet, I., Very-high-order WENO schemes, *47th AIAA Aerospace Sciences Meeting including the New Horizons Forum and Aerospace Exposition*, 2009.
[2] Diot, S., Clain, S., Loubère, R., Improved detection criteria for the Multi-dimensional Optimal Order Detection (MOOD) on unstructured meshes with very high-order polynomials, *Computers and Fluids*, 64, 2012, 43-63.
[3] Clain, S., Machado, G. J., A very high-order finite volume method for the time-dependent convection-diffusion problem with Butcher Tableau extension, *Computers and Mathematics with Applications*, 68, 2014, 1292-1311.
[4] Fu, L., Very-high-order TENO schemes with adaptive accuracy order and adaptive dissipation control, *Computer Methods in Applied Mechanics and Engineering*, 387, 2021, 114193.
[5] Shen, Y., Zha, G., Large eddy simulation using a new set of sixth order schemes for compressible viscous terms, *Journal of Computational Physics*, 229, 2010, 8296-8312.
[6] Chun, C., Neta, B., A new sixth-order scheme for nonlinear equations, *Applied Mathematics Letters,* 25, 2012, 185-189.
[7] Clain, S., Machado, G. J., Nóbrega, J. M., Pereira, R. M. S., A sixth-order finite volume method for multidomain convection-diffusion problem with discontinuous coefficients, *Computer Methods in Applied Mechanics and Engineering*, 267, 2013, 43-64.
[8] Boularas, A., Clain, S., Baudoin, F., A sixth-order finite volume method for diffusion problem with curved boundaries, *Applied Mathematical Modelling*, 42, 2017, 401-422.
[9] Costa, R., Clain, S., Machado, G. J., A sixth-order finite volume scheme for the steady-state incompressible Stokes equations on staggered unstructured meshes, *Journal of Computational Physics*, 349, 2017, 501-527.
[10] Sharma, N., Sengupta, A., Rajpoot, M., Samuel, R. J., Sengupta, T. K., Hybrid sixth order spatial discretization scheme for non-uniform Cartesian grids, *Computers and Fluids,* 157, 2017, 208-231.
[11] Boersma, B. J., A 6th order staggered compact finite difference method for the incompressible Navier-Stokes and scalar transport equations, *Journal of Computational Physics*, 230, 2011, 4940-4954.
[12] Clain, S., Diot, S., Loubère, R., Multi-dimensional Optimal Order Detection (MOOD) - a Very High-Order Finite Volume Scheme for Conservation Laws on Unstructured Meshes, *Springer Proceedings in Mathematics*, 4, 2011, 263-271.
[13] Wu, C., Wu, L., Li, H., Zhang, S., Very high order WENO schemes using efficient smoothness indicators, *Journal of Computational Physics*, 432, 2021, 110158.
[14] Jiang, Y., Mao, M., Deng, X., Liu, H., Large eddy simulation on curvilinear meshes using seventh-order dissipative compact scheme, *Computers and Fluids*, 104, 2014, 73-84.
[15] Mazaheri, A., Nishikawa, H., Very efficient high-order hyperbolic schemes for time-dependent advection-diffusion problems: Third-, fourth-, and sixth-order, *Computers and Fluids*, 102, 2014, 131-147.
[16] Fu, L., A very-high-order TENO scheme for all-speed gas dynamics and turbulence, *Computer Physics Communications*, 244, 2019, 117-131.
[17] Vasconcelos, A. G. R., Albuquerque, D. M. S., Pereira, J. C. F., A very high-order finite volume method based on weighted least squares for elliptic operators on polyhedral unstructured grids, *Computers and Fluids*, 181, 2019, 383-402.
[18] Coudière, Y., Turpault, R., Very high order finite volume methods for cardiac electrophysiology, *Computers and Mathematics with Applications*, 74, 2017, 684-700.
[19] Coudière, Y., Turpault, R., A domain decomposition strategy for a very high-order finite volumes scheme applied to cardiac electrophysiology, *Journal of Computational Science*, 37, 2019, 101025.
[20] Bai, Z., Zhong, X., New very high-order upwind multi-layer compact (MLC) schemes with spectral-like resolution for flow simulations, *Journal of Computational Physics*, 378, 2019, 63-109.
[21] Gaburro, E., Boscheri, W., Chiocchetti, S., Klingenberg, C., Springel, V., Dumbser, M., High order direct Arbitrary-Lagrangian-Eulerian schemes on moving Voronoi meshes with topology changes, *Journal of Computational Physics*, 407, 2020, 109167.
[22] Tsoutsanis, P., Dumbser, M., Arbitrary high order central non-oscillatory schemes on mixed-element unstructured meshes, *Computers and Fluids*, 225, 2021, 104961.
[23] Guo, Y., Shi, Y. F., Li, Y. M., A fifth-order finite volume weighted compact scheme for solving one-dimensional Burgers' equation, *Applied Mathematics and Computation*, 281, 2016, 172-185.
[24] Xu, M., A high order scheme for unsteady heat conduction equations, *Applied Mathematics and Computation*, 348, 2019, 565-574.
[25] Costa, P. M. P., Albuquerque, D. M. S., A novel approach for temporal simulations with very high-order finite volume schemes on polyhedral unstructured grids, *Journal of Computational Physics*, 453, 2022, 110960.
[26] Ramírez, L., Edreira, L., Couceiro, I., Ouro, P., Nogueira, X., Colominas, I., A new Mean Preserving Moving Least Squares method for Arbitrary Order Finite Volume schemes, *Applied Mathematics and Computation*, 443, 2023, 127768.
[27] Dell'Accio, F., Di Tommaso, F., Nudo, F., Generalizations of the constrained mock-Chebyshev least squares in two variables: Tensor product vs total degree polynomial interpolation, *Applied Mathematics Letters*, 125, 2022, 107732.
[28] Dell'Accio, F., Marcellán, F., Nudo, F., An extension of a mixed interpolation–regression method using zeros of orthogonal polynomials, *Journal of Computational and Applied Mathematics*, 450, 2024, 116010.
[29] Dell'Accio, F., Nudo, F., Polynomial approximation of derivatives through a regression–interpolation method, *Applied Mathematics Letters*, 152, 2024, 109010.
[30] Prasopchingchana, U., Manewattana, T., A new scheme for the finite volume method verified with two dimensional laminar natural convection in a square cavity, *Engineering Journal*, 19, 2015, 133-152.
[31] Prasopchingchana, U., Modification of the Lagrange Interpolating Polynomial Scheme for Using with the Finite Difference Method, *MATEC Web Conf.*, 136, 01005, 2017.
[32] Frank P. Incropera, David P. Dewitt, Theodore L. Bergman, Lavine, A. S., *Fundamentals of heat and mass transfer*, John Wiley & Sons (Asia) Pte. Ltd., 2007.
[33] Botella, O., Peyret, R., Benchmark spectral results on the lid-driven cavity flow, *Computers and Fluids*, 27, 1998, 421-433.
[34] Bruneau, C. H., Saad, M., The 2D lid-driven cavity problem revisited, *Computers and Fluids*, 35, 2006, 326-348.
[35] De Vahl Davis, G., Natural convection of air in a square cavity: A bench mark numerical solution, *International Journal for Numerical Methods in Fluids*, 3, 1983, 249-264.
[36] Markatos, N. C., Pericleous, K. A., Laminar and turbulent natural convection in an enclosed cavity, *International Journal of Heat and Mass Transfer*, 27, 1984, 755-772.
[37] Saitoh, T., Hirose, K., High-accuracy bench mark solutions to natural convection in a square cavity, *Computational Mechanics*, 4, 1989, 417-427.
[38] Le Quéré, P., Accurate solutions to the square thermally driven cavity at high Rayleigh number, *Computers and Fluids*, 20, 1991, 29-41.
[39] Barakos, G., Mitsoulis, E., Assimacopoulos, D., Natural convection flow in a square cavity revisited: Laminar and turbulent models with wall functions, *International Journal for Numerical Methods in Fluids*, 18, 1994, 695-719.
[40] Dixit, H. N., Babu, V., Simulation of high Rayleigh number natural convection in a square cavity using the lattice Boltzmann method, *International Journal of Heat and Mass Transfer*, 49, 2006, 727-739.
[41] Baïri, A., Nusselt-Rayleigh correlations for design of industrial elements: Experimental and numerical investigation of natural convection in tilted square air filled enclosures, *Energy Conversion and Management*, 49, 2008, 771-782.
[42] Zhao, B., Tian, Z., High-resolution high-order upwind compact scheme-based numerical computation of natural convection flows in a square cavity, *International Journal of Heat and Mass Transfer*, 98, 2016, 313-328.

[43] ElSherbiny, S. M., Raithby, G. D., Hollands, K. G. T., Heat transfer by natural convection zcross vertical and inclined air layers, *Journal of Heat Transfer*, 104, 1982, 96-102.
[44] Zhu, Z. J., Yang, H. X., Numerical investigation of transient laminar natural convection of air in a tall cavity, *Heat and Mass Transfer/Waerme- und Stoffuebertragung*, 39, 2003, 579-587.
[45] Báez, E., Nicolás, A., From cats eyes to multiple disjoint natural convection flow in tall tilted cavities: A direct primitive variables approach, *Physics Letters, Section A: General, Atomic and Solid State Physics*, 377, 2013, 2270-2274.
[46] Ghia, U., Ghia, K. N., Shin, C. T., High-Re solutions for incompressible flow using the Navier-Stokes equations and a multigrid method, *Journal of Computational Physics*, 48, 1982, 387-411.
[47] Erturk, E., Corke, T. C., Gökçöl, C., Numerical solutions of 2-D steady incompressible driven cavity flow at high Reynolds numbers, *International Journal for Numerical Methods in Fluids*, 48, 2005, 747-774.
[48] Xu, L., Chen, R., Scalable parallel finite volume lattice Boltzmann method for thermal incompressible flows on unstructured grids, *International Journal of Heat and Mass Transfer*, 160, 2020, 120156.
[49] Zhao, Z., Wen, M., Li, W., A coupled gas-kinetic BGK scheme for the finite volume lattice Boltzmann method for nearly incompressible thermal flows, *International Journal of Heat and Mass Transfer*, 164, 2021, 120584.
[50] Reyes Barraza, J. A., Deiterding, R., A curvilinear lattice Boltzmann scheme for thermal flows, *Mathematics and Computers in Simulation*, 202, 2022, 405-420.

ORCID iD

Uthai Prasopchingchana https://orcid.org/0000-0002-0857-7870

How to cite this article: Prasopchingchana U. A Very High-Order Spatial Lagrange Interpolating Polynomial Scheme, *J. Appl. Comput. Mech.*, 11(3), 2025, 844-860. https://doi.org/10.22055/jacm.2024.47901.4824